

Interfacial Segregation of Alloying Elements During Dissimilar Ultrasonic Welding of AA6111 Aluminum and Ti6Al4V Titanium



CHAOQUN ZHANG, JOSEPH D. ROBSON, SARAH J. HAIGH,
and PHILIP B. PRANGNELL

Ultrasonic welding is a promising technique for joining dissimilar metals. A particular metal combination of interest to the automotive industry is aluminum-titanium. In such welds, performance is often controlled by processes at the interface, including segregation and intermetallic precipitate formation. This study used high-resolution electron microscopy to investigate this in detail. Enrichment of silicon, magnesium, and oxygen were found at ultrasonic welded aluminum/titanium interfaces; however, other alloying elements such as copper and V were not segregated. Surprisingly, in a very short welding time (1.4 seconds), ~ 4 at. pct of Si was found at the Al/Ti interface. The segregated Si distribution varied inversely with that of O and Mg. The residual oxides and the segregated Si on the Al/Ti interface may act as a barrier for Al₃Ti nucleation and growth. The strong chemical attraction between Ti and Si is probably the driving force for Si segregation to the Al/Ti interface. The presence of discontinuous oxides at the Al/Ti weld interface may deteriorate the mechanical properties of the weld.

<https://doi.org/10.1007/s11661-019-05395-7>
© The Author(s) 2019

I. INTRODUCTION

ULTRASONIC welding (UW) has been widely used for joining dissimilar metals, such as Al-Mg,^[1–3] Al-Steel,^[4–6] Al-Cu,^[7] and Al-Ti^[8,9] because its low welding temperature and low energy input avoid the formation of a thick and brittle intermetallic layer at the weld interface. Although the energy input of UW is quite low, brittle intermetallic compounds (IMC) have still often been observed at weld interfaces.^[1,4,10–12] Once the coverage and thickness of the IMC layer exceeds a certain level, it becomes detrimental to the mechanical properties of the welded interface.^[13] Thus, many studies have investigated IMC formation and growth on dissimilar metal interfaces.^[1,3,10,12,14] However, elemental segregation at dissimilar metal interfaces has received less attention, although this could also have an important influence on a weld's mechanical properties and on IMC growth. Fuji

et al.^[13] have studied segregation for friction welded titanium-to-aluminum interfaces using transmission electron microscopy (TEM) and energy dispersive X-ray spectroscopy (EDS) elemental analysis. They observed an Al₃Ti IMC layer formed on the weld interface as well as more than 20 at. pct Si segregated to the interface between the Al₃Ti intermetallic phase particles and the titanium base metal. The aluminum component of the weld contained silicon and the authors proposed that the Si segregation at the interface retarded the growth of the Al₃Ti intermetallic layer by acting as a barrier layer for diffusion.^[13] In addition, the Al-Ti weld with Si segregation showed better mechanical properties (bend angle)^[13] for an identical heat treatment time compared with Al-Ti welds without Si segregation. However, in Fuji *et al.*'s study^[13] (year: 1995), Si segregation was only detected at Al-Ti weld interfaces after heat treatment (873 K, 1 hour and 873 K, 0.1 hour), and no interface Si segregation was observed in the as-welded Al-Ti condition. Therefore, it is still unknown whether silicon or other important alloying elements in aluminum alloys (*e.g.*, Cu, Mg) and titanium alloys (*e.g.*, V) can segregate to the weld interfaces in the short process times associated with solid-state welding processes (*e.g.*, friction welding, friction stir welding, and UW). Furthermore, the dispersion of the surface oxide layers on Al and Ti base metals during UW is also of great interest to the quality of the weld and has not been studied in detail. In this paper, we apply scanning transmission

CHAOQUN ZHANG is with the Shanghai Key Laboratory of Digital Manufacture for Thin-Walled Structures, School of Mechanical Engineering, Shanghai Jiao Tong University, Shanghai, 200240, P.R. China and also with the School of Materials, University of Manchester, Manchester, UK. Contact e-mails: chaoqunzhang@sjtu.edu.cn, acezqc@gmail.com JOSEPH D. ROBSON, SARAH J. HAIGH, and PHILIP B. PRANGNELL are with the School of Materials, University of Manchester.

Manuscript submitted April 12, 2019.

Article published online September 3, 2019

electron microscope (STEM) imaging and nanoscale EDS elemental mapping to investigate the distribution of all alloying elements and oxides at the as-welded UW aluminum-titanium interfaces, providing higher resolution microstructural characterization than has been previously reported.

II. MATERIAL AND METHODS

Thin 6111-T4 aluminum alloy sheets ($25 \times 75 \times 0.93$ mm) and TiAl6V4 titanium sheets ($25 \times 75 \times 1$ mm) were used for UW in the present study. AA6111 represents the 6xxx aluminum alloy class of technological interest to the automotive industry. A welding time of 1.4 seconds, welding energy of 1967 J, and welding pressure 0.55 MPa were used to produce the AA6111/Ti6Al4V joints. The welds produced were lap spot welds, with the AA6111 sheet on the upper side. The details of the weld macro appearance and the schematic diagram of the UW process can be found in Reference 8. An FEI QUANTA 3D Focused Ion Beam Milling (FIB) system was used for preparing thin foils for transmission electron microscopy (TEM) observation. The system was operated at 30 kV for rough cutting and milling, and 5 and 2 kV for final polishing. The position where the TEM specimens were extracted was shown in a previous paper.^[8] Typical Al/Ti interface regions (~ 1000 nm \times 1500 nm) on the FIB-thinned TEM specimens were selected for STEM-EDS analysis using an FEI Titan G2 80 to 200 scanning transmission electron microscope with ChemiSTEM™ technology. A 0.5 nA probe current, a convergence semi-angle of 21 mrad, a 200 kV accelerating voltage, and an HAADF inner semi-angle of 54 mrad were used during operation of the Titan STEM instrument. This instrument has four windowless silicon drift detectors (SDD) integrated into the objective lens (total EDS collection angle = 0.7 srad) and the windowless EDS detector design considerably enhances the detection of the characteristic X-rays of light elements, such as oxygen. The high-brightness X-FEG electron source and the four SDD EDS detectors enable the instrument to have a spatial resolution of better than 0.1 nm for imaging and elemental analysis, with a high signal-to-noise ratio. For example, the ChemiSTEM™ technology can realize atomic oxygen mapping in a Sr and Ti oxide crystal.^[15] For acquiring EDS data, a 30- μ s pixel dwell time and a total acquisition time of 15 to 20 minutes was used. An absorption-corrected Cliff–Lorimer approach within the Bruker Esprit software was used for performing semi-quantitative analysis of the EDS data. The TEM specimen thickness was assumed to be 100 to 200 nm.

III. RESULTS AND DISCUSSION

A. Si Segregation on Al/Ti Interface

During the UW process, the Al/Ti interface (AA6111/Ti6Al4V) experienced a 1.4-second welding cycle, with a ~ 520 °C peak temperature and severe cyclic high

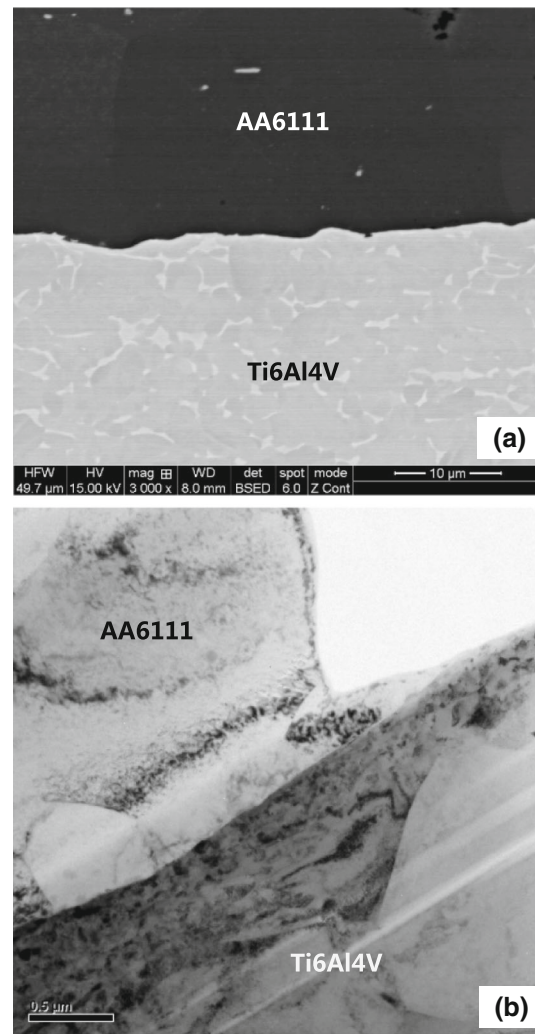
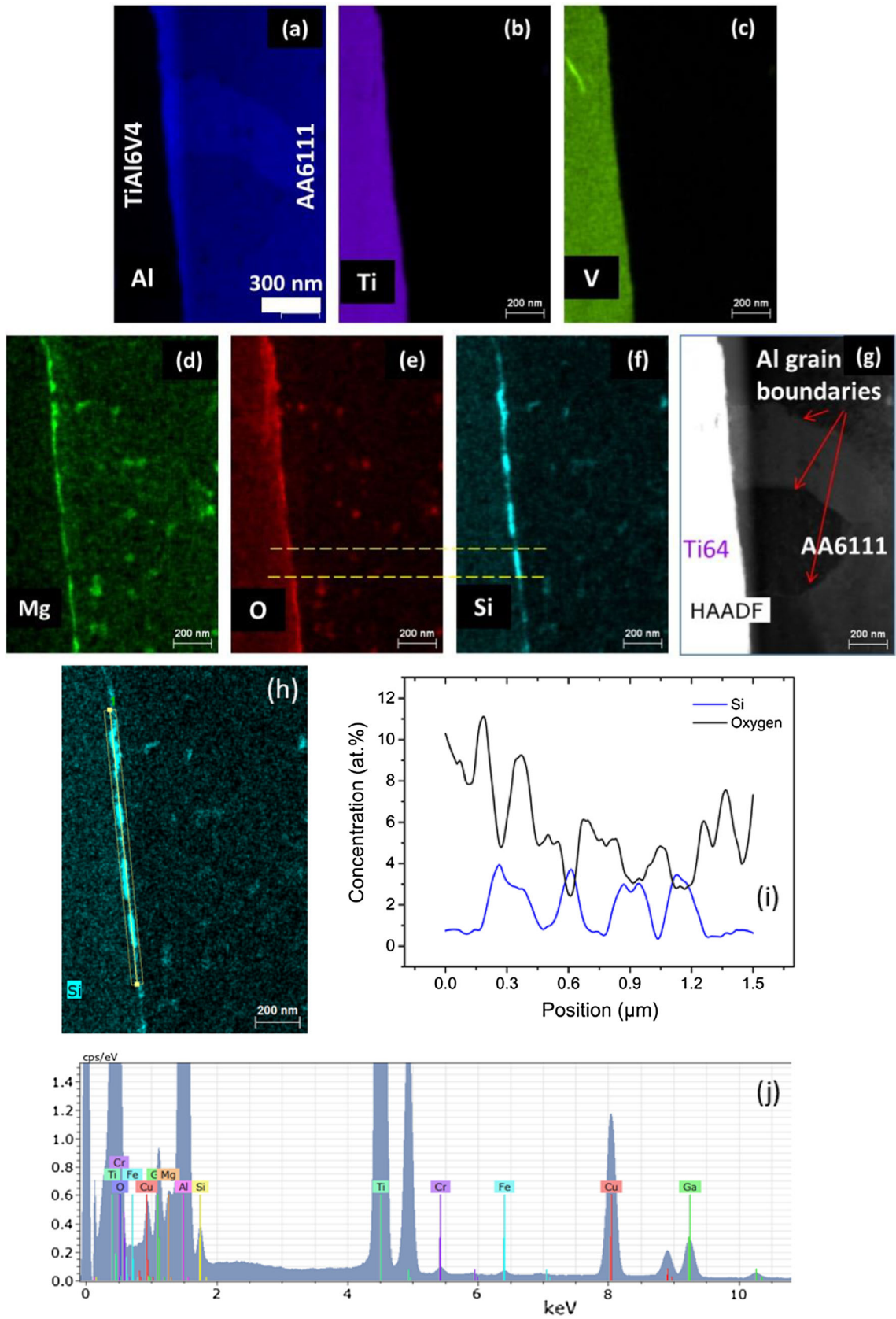


Fig. 1—SEM and TEM images of typical AA6111–Ti6Al4V ultrasonic spot welded interface (welding time: 1.4 s, welding energy: 1967 J). (a) SEM BSE image, (b) TEM bright field image.

strain rate plastic deformation.^[8] In the as-welded condition, no IMC layer was observed on the Al/Ti interface (Figures 1 and 2.^[8]). However, interestingly, Si, Mg, and O enrichment were detected at the interface using STEM-EDS spectrum imaging, as shown in Figures 2 and 3. Surprisingly, in such a short welding time (1.4 seconds), ~ 4 at. pct of Si was found segregated to the Al/Ti interface (Figure 4). This segregation level is much higher than the concentration in the AA6111 base metal, 0.85 pct. According to a previous study, Si enrichment on the surface of the as-received Al alloys is

Fig. 2—STEM-EDS elemental maps at the AA6111/Ti6Al4V interface region. (a) Al map, (b) Ti map, (c) V map, (d) Mg map, (e) O map, (f) Si map, (g) STEM-HAADF image, (h) Si map with the linescan region overlaid (the bright yellow rectangle), (i) Si and O distribution along the interface, (j) sum spectra of the whole region. (Semi-quantitative analysis, when quantifying the EDS data, the following elements were included: Cu, Mg, Al, Si, Fe, Ti, V, O, Ga, Cf, Ge, Zr; quantification of the linescan was achieved by averaging along the interface over 10 spectral points) (Color figure online).



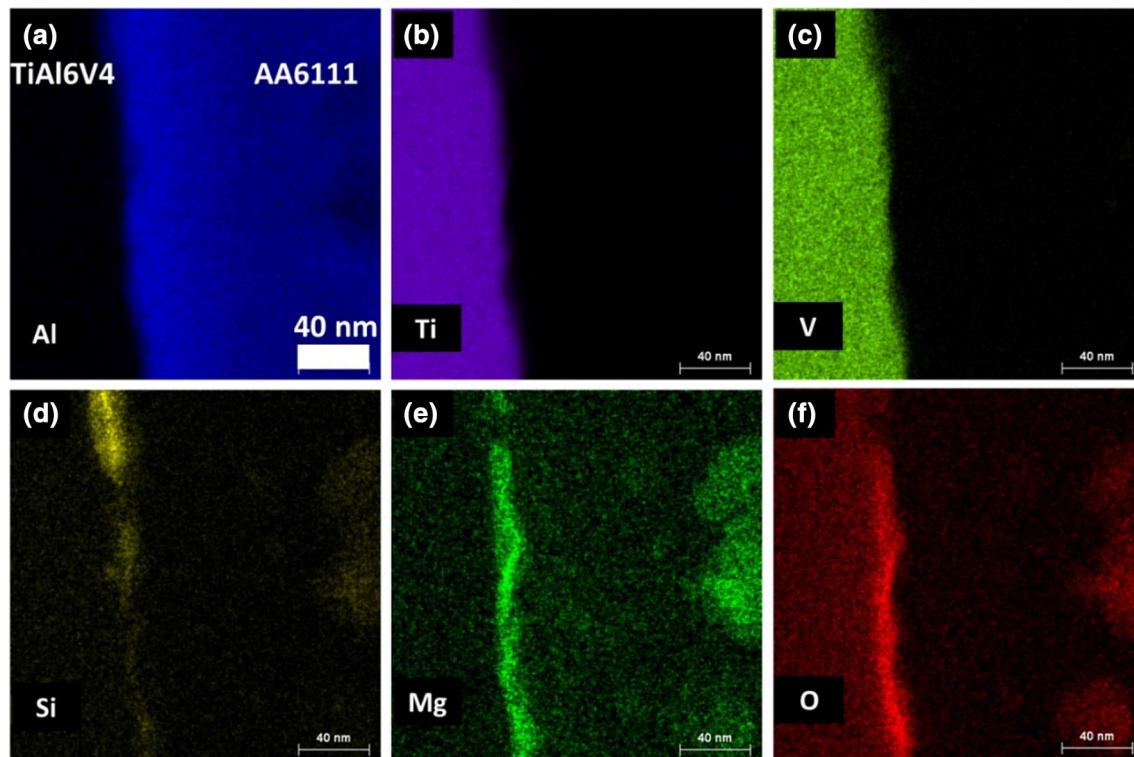


Fig. 3—STEM-EDS element maps in the AA6111/Ti6Al4V interface region, (a) Al map, (b) Ti map, (c) V map, (d) Si map, (e) Mg map, (f) O map.

also not expected.^[16] This suggests that the measured Si enrichment on the Al/Ti interface (Figures 2 and 3) was formed during the ultrasonic welding process, with Si originally from the interior of AA6111 alloy base metal.

This high local Si concentration was formed in a very short welding time (just 1.4 seconds), which suggests that Si diffusion in the Al alloy during ultrasonic welding process may be greater than expected. In UW, high strain rate severe plastic deformation (SPD) has been previously reported to enhance diffusivity by injecting an enhanced vacancy flux near the weld interface.^[17] The measured concentration of Si segregation (~ 4 at. pct) found in the present study was, however, lower than that previously reported by TEM-EDS^[13] in an Al/Ti joint after post-weld heat treatment at 600 °C for 1 hour, which measured levels as high as 20 at. pct Si segregation. In Reference 13, the Al base metal only contained 0.12 pct Si, which is much less than the concentration of 0.85 pct Si in the AA6111 aluminum alloy used in the present study. This indicates that the Si segregation on the Al/Ti interface may not have reached saturation equilibrium during the very short UW process. The reason for Si segregation to the Al/Ti interface is likely to be that the affinity between Si atoms and Ti atoms is very strong, stronger than the affinity between Si atoms and Al atoms.^[18,19] The driving force for Si segregation will be discussed further in Section III–E.

From Figures 2(e), (f), and (i), it can be seen that the distribution of silicon on the Al/Ti interface was discontinuous; notably its distribution is largely inverse to that of oxygen and magnesium. This could be because

the broken oxide film (containing both magnesium oxide and aluminum oxide) at the Al/Ti interface acts as a barrier, which prevents direct contact between AA6111 alloy and Ti6Al4V alloy, so that the attraction of Ti to Si atoms in AA6111 was blocked. It should also be noted that the observed Si distribution was not absolutely inverse to that of oxygen and magnesium because with a 100-nm-thick foil, there could be Si enriched below or above the residual oxide fragments in the thickness direction of the TEM specimen.

Furthermore, as shown in Figure 2, no Si segregation was detected on the grain boundaries of AA6111 near the Al/Ti interface. This suggests that the driving force for Si segregation to the Al/Ti interface is much higher than that for Si segregation to AA6111 grain boundaries.

The segregated Si to the Al/Ti interface could act as a barrier between Al and Ti, which could slow down the interdiffusion of Al and Ti and reduce titanium aluminide formation as interdiffusion is the prerequisite for Al-Ti intermetallic nucleation. Thus, this could be one reason for the observation of a lack of an IMC layer at the Al-Ti interface. A much slower IMC layer growth rate was also observed by Fuji *et al.* due to the presence of Si at the interface.^[13]

B. Mg and O on Al/Ti Interface

From the quantified Mg and O profiles (Figure 5) across the Al/Ti interface, it can be seen there was also approximately 5.5 at. pct Mg segregated to the Al/Ti interface, which is again much more than that is present

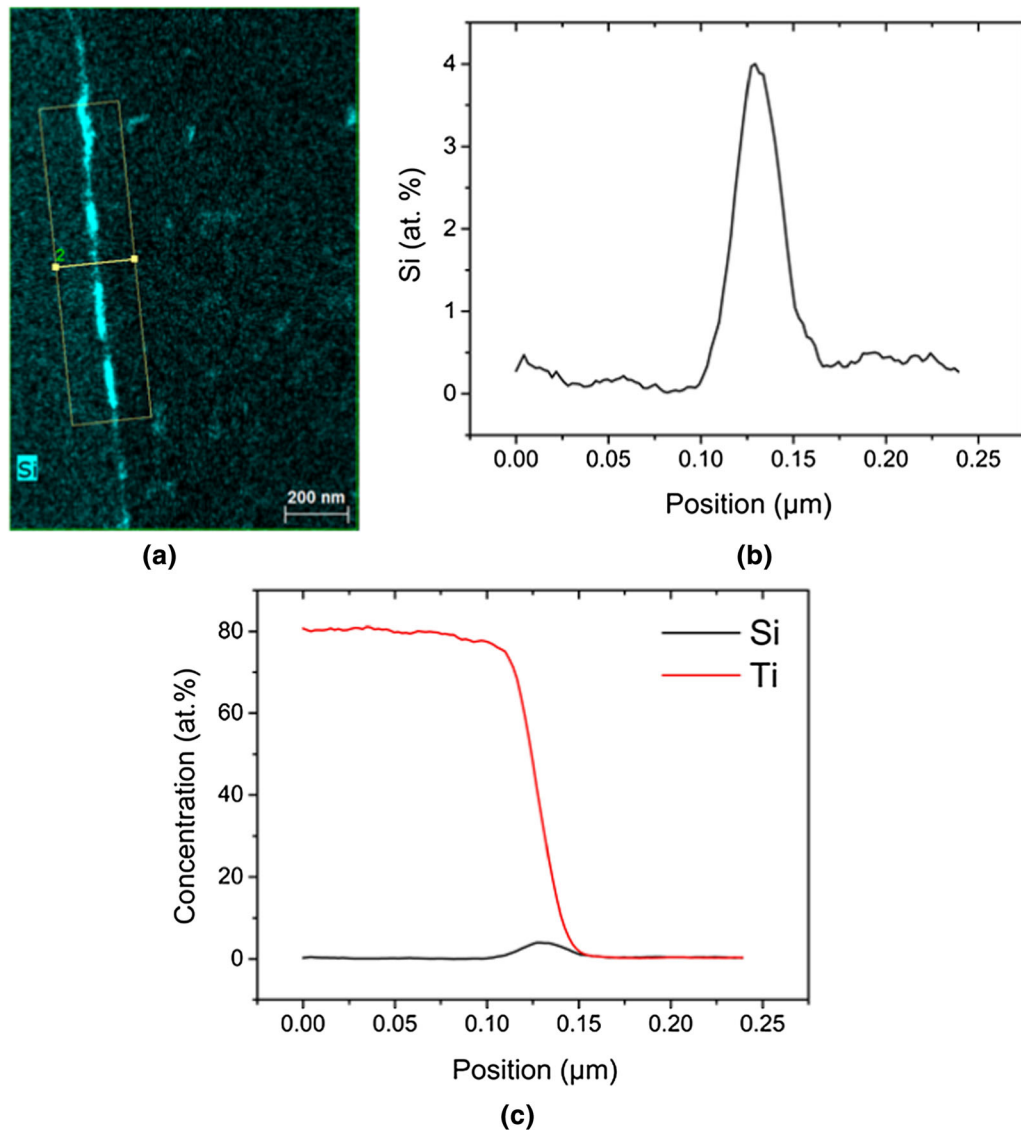


Fig. 4—STEM-EDS line scan across the Si-rich region on the Al/Ti interface in the same region shown in Fig. 2, (a) STEM-EDS Si map, (b) the Si concentration profile across the interface, (c) the Ti and Si concentration profile across the interface (in the same region with Fig. 2, semi-quantitative analysis, when quantifying the EDS data, the following elements were included: Cu, Mg, Al, Si, Fe, Ti, V, O, Ga, Cf, Ge, Zr; quantification of the linescan was achieved by averaging vertically and horizontally with 3 spectral points per pixel quant).

in the AA6111 Al base metal (0.75 pct). However, this was generally in association with oxygen, with more than 18 at. pct oxygen found at the interface, suggesting that in addition to magnesium oxides, there could also be complex aluminum, magnesium/titanium oxides present at the interface.

According to previous investigations,^[20–23] for commercial aluminum sheet alloys containing Mg, Mg strongly segregates to the surface to become incorporated in the oxide film and the segregation concentration can reach over 10 at. pct. Bloch *et al.* also found that Mg segregation on the surface of Al alloys greatly enhanced the oxygen adsorption rate at room temperature.^[22] Hence, most of the observed Mg and O “enrichment” on the Al/Ti interface probably pre-existed in the form of the oxide film present on the surface of AA6111 before ultrasonic welding. In

addition, preferential oxidation of Mg is expected due to its high activity and could be further increased in the initial abrasion stages of UW, due to the heat generation and the breaking of the original surface oxide layer by the severe friction in UW, *i.e.*, as a result of the exposure of fresh surface generated under the aggressive UW contact conditions before forming a metallurgical joint. For example, Field *et al.*^[24] have found that thick layers of Mg oxide form rapidly on the surface of Al-Mg alloys at temperatures higher than 377 °C. As we have previously measured,^[8,9] the peak temperature during Al/Ti ultrasonic welding can reach in excess of 450 °C, which could allow rapid formation of Mg oxide on the surface.

Figures 2 and 3 also confirm that the distribution of Mg on the Al/Ti interface is coincident with that of oxygen, consistent with the presence of magnesium

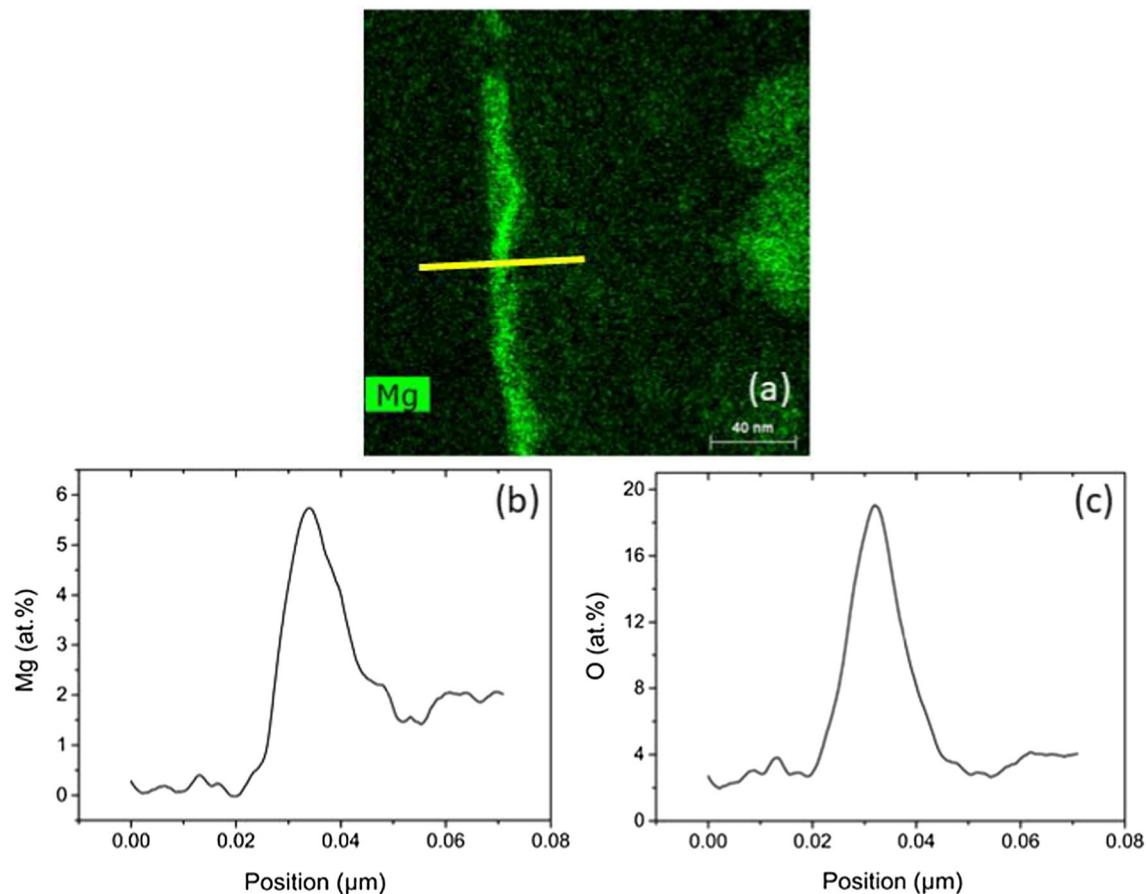


Fig. 5—STEM-EDS line scan across the Mg-rich region on the Al/Ti interface, (a) STEM-EDS Mg map, (b) the Mg concentration profile across the interface, (c) the O concentration profile across the interface. (in the same region with Fig. 3, semi-quantitative analysis, when quantifying the EDS data, the following elements were included: Cu, Mg, Al, Si, Fe, Ti, V, O, Ga, Cf, Ge, Zr; quantification of the linescan was achieved by averaging parallel to the interface).

oxide (or O-rich Mg) originally on the surface of the AA6111 alloy, prior to metallurgical bonding. In addition, the discontinuous distribution of the magnesium oxide suggests that the original surface oxide layer has not been totally removed by the ultrasonic welding process, but was only broken into pieces, as illustrated in Figure 6. The reason for the surface oxide layer not being totally removed could be that the amplitude of ultrasonic vibration is very small (only $\sim 6 \mu\text{m}$) compared with the 10 mm wide welded region. A residual oxide layer has also been experimentally observed by Magin and Balle at an ultrasonically welded Al-Ti interface using TEM-Electron energy loss spectroscopy (EELS),^[25] and the presence of an oxide layer at the interface in various Al-Ti diffusion couples has also been suggested by some previous investigators.^[26,27]

The discontinuous residual oxides (including Mg oxides) on the Al/Ti interface could retard the formation and growth of the Al-Ti reaction intermetallic layer and, consequently, could be another reason for the lack of the formation of a visible IMC layer at the Al-Ti weld interface, as observed in our previous paper.^[8] The effect of the residual oxide layer on the IMC layer growth after prolonged heat treatment will be discussed in a forthcoming paper.

Apart from retarding IMC layer growth, the residual discontinuous oxide layer at the Al/Ti weld interface would prevent direct contact between Al and Ti and could potentially negatively affect the final weld mechanical properties. Similarly, residual discontinuous oxides have also often been observed in a similar solid-state joining process, friction stir welding.^[28–31] Here they have been found to influence the fracture path after heat treatment^[29] with crack initiation also having been observed to occur along the residual oxide layer.^[31]

C. Discussion of the Composition of the Si-Rich Layer

The observed thickness of the Si-enriched layer was ~ 20 to 40 nm (Figure 4), and the maximum concentration of silicon was in excess of 4 at. pct. This is far in excess of the maximum solubility of Si in either Al or Ti, and thicker than expected for segregation to a discrete interface, meaning that either some silicon precipitation or intermetallic phase formation may be expected at the interface. The morphology of the Si segregation (Figures 2 and 3) also suggests there may be a discrete phase present at the interface, rather than just a segregation layer. The binary Ti-Si phase diagram^[32] shows that in the composition range of interest, Ti_5Si_3 is the most

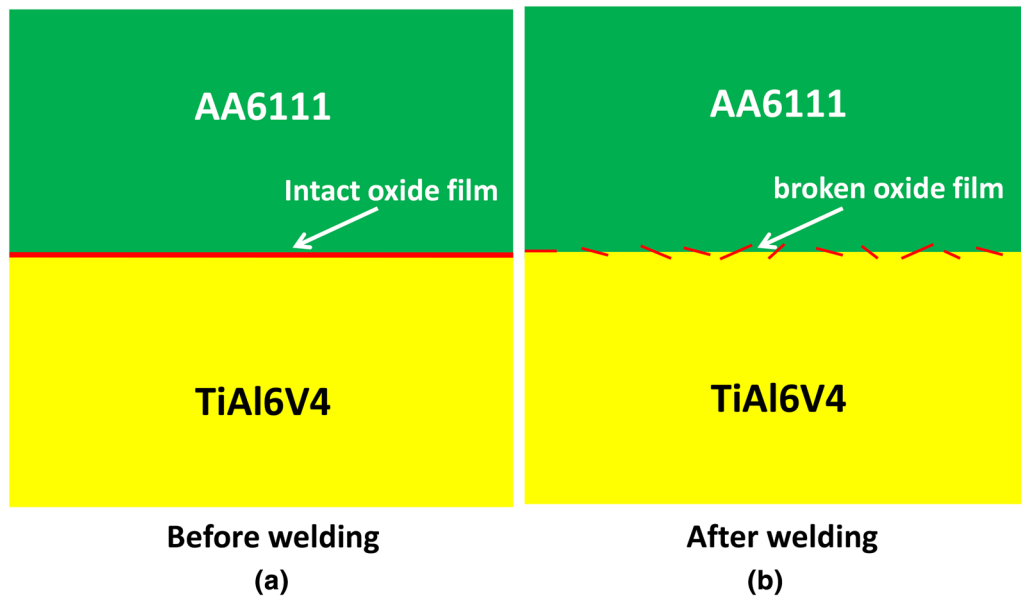


Fig. 6—Schematic diagram of intact oxide films (long red line) on AA6111 and Ti6Al4V surface before UW (a) and broken oxide film (short red lines) on interface after UW (b) (Color figure online).

stable intermetallic phase. However, which phase is observed in practice will also depend on kinetic factors and, in particular, the activation energy for nucleation. It has been shown that the activation energy for the formation of TiSi_2 (165.4 kJ/mol) is much lower than that of Ti_5Si_3 (205.2 kJ/mol),^[33] which means TiSi_2 could form more rapidly than Ti_5Si_3 under the highly transient low-temperature conditions seen in ultrasonic welding. For example, at temperatures below 1270 °C, Yeh *et al.*^[33] found that in the solid-state reaction between Ti and Si, TiSi_2 was the dominant final product, rather than Ti_5Si_3 . To experimentally identify the Si-rich phase, we have attempted to obtain quantified line scans of both Si and Ti across the Si-rich phase region (Figure 4). However, due to the limitations of the TEM specimen and EDS analysis, it was difficult to accurately determine the chemical composition of the very tiny Si-rich particles seen in Figure 4(a), as the interaction volume of the incident electron beam through the foil thickness was larger than the size of the nanoscale Si-rich particles. As a result, the characteristic X-rays of the surrounding material were also captured when scanned over the Si-rich phase position. Therefore, to more accurately identify the Si-rich phase high-resolution crystallographic analysis will be necessary in the future.

D. Discussion of Si Segregation Kinetics

The accumulation of silicon at the interface requires diffusion from its source in the aluminum alloy and it is therefore of interest to estimate whether a simple diffusion calculation, based on mass balance, and Fick's first law can explain the very rapid attainment of the enhanced silicon concentration observed after UW. Based on the experimental observations, a 20-nm wide silicon-enriched region was considered in this analysis. It was assumed the initial concentration of silicon at the

interface was 0.85 pct, which corresponds to the silicon content of the aluminum matrix. The mass balance, as described in Eq. [1], requires that the amount of silicon gained in the interface layer must be equal to the amount removed from the aluminum matrix. In the common approximation of a linear concentration gradient, mass balance gives the following relationship:

$$(C_{\text{Si}}^i - \bar{C}_{\text{Si}}) \cdot w = \frac{\bar{C}_{\text{Si}}}{2} \cdot x_{\text{D}}, \quad [1]$$

where C_{Si}^i is the silicon concentration in the interface layer, \bar{C}_{Si} is the silicon concentration in the aluminum matrix, 0.85 at. pct, w is the width of the silicon-enriched region, assumed to be a constant value 20 nm, and x_{D} is the required diffusion distance of Si in the aluminum matrix to attain the final concentration at the interface, C_{Si}^i . The diffusion distance of Si in the aluminum matrix is approximated by $x_{\text{D}} = 2\sqrt{D \cdot t}$, where D ($2.6 \times 10^{-9} \text{ cm}^2/\text{s}$) is the diffusion coefficient of Si^[34] in an aluminum matrix at 520 °C (~ the peak welding temperature), and t is the time at the peak welding temperature. Using this approximation, the relationship between the time over which diffusion occurs (t) and the silicon concentration (C_{Si}^i) in the interface layer can be calculated, as shown in Figure 7.

Figure 7 demonstrates the very rapid increase in Si concentration at the interface that is possible by diffusion at the peak temperature reached during welding. As shown in Figure 7, only 0.02 s at the peak welding temperature of 520 °C is needed to reach the measured concentration of silicon at the interface (~ 4 at. pct). Although this analysis quite simplistic, and assumes the capacity of the interface to absorb Si is not limited, it is sufficient to demonstrate that it is feasible for Si to enrich to the measured level during the weld thermal cycle (where the material is close to the peak

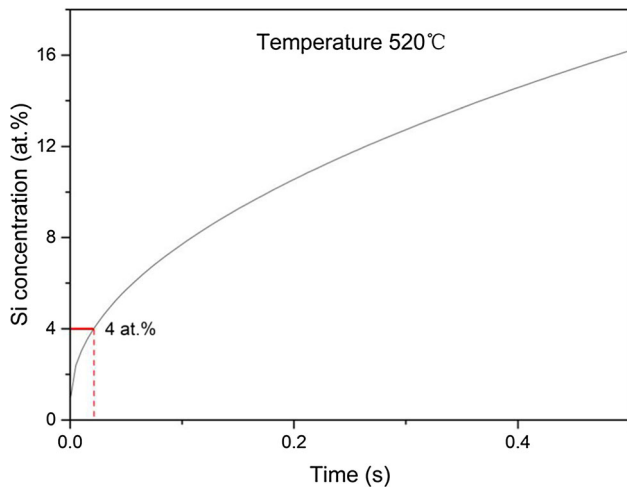


Fig. 7—The calculated relationship between diffusion time and silicon concentration at the interface layer (for a temperature corresponding to the peak welding temperature of 520 °C).

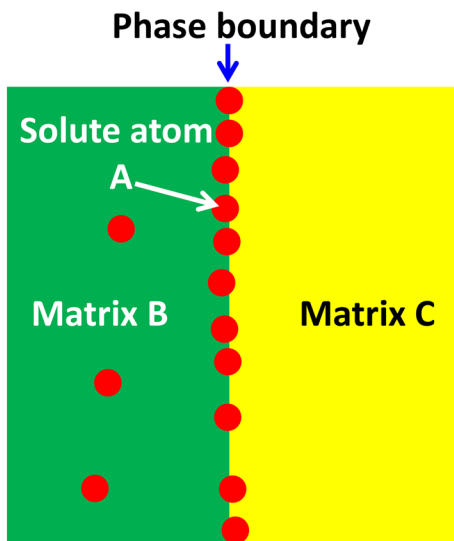


Fig. 8—Schematic diagram of segregation of solute atom A in matrix B to matrix B/matrix C interface.

temperature for durations of ~ 0.4 seconds^[8]). These estimates therefore suggest that the enhanced deformation-induced diffusion reported to occur in the interface region for UW is not necessary to obtain the level of Si interface segregation observed.

E. Discussion of the Driving Force for Segregation

Next we will examine the driving force necessary for interface segregation to occur. According to thermodynamic theory, the greater the absolute value of negative enthalpy chemical of mixing ($\Delta H_{X-Y}^{\text{mix}}$) between an element X and element Y, the more chemical attraction there is between them. Thus, in the case of present study, for solute atom A in matrix B, if the negative value of chemical enthalpy of mixing between A and the other matrix C ($\Delta H_{A-C}^{\text{mix}}$) (which shares an interface with matrix B) is smaller than $\Delta H_{A-B}^{\text{mix}}$, solute atom A will segregate to the matrix B/matrix C interface, which leads to lower system free energy, as illustrated in Figure 8.

The enthalpies of chemical mixing $\Delta H_{X-Y}^{\text{mix}}$ between the alloying elements (Si, V, Cu, Mg, Fe) and the matrices (Al, Ti) reported in the literature are listed in Table I.

It can be seen that in all combinations, $\Delta H_{\text{Ti-Si}}^{\text{mix}}$ has the lowest value (-66 kJ/mol), and much lower than that of $\Delta H_{\text{Al-Si}}^{\text{mix}}$ (-19 kJ/mol). Thus, there is a strong driving force for Si to segregate to the Al/Ti interface from the AA6111 base metal.

In comparison, for V, $\Delta H_{\text{Ti-V}}^{\text{mix}}$ is much lower than $\Delta H_{\text{Al-V}}^{\text{mix}}$, so V in Ti6Al4V is not expected to segregate to the Al/Ti interface, which is in agreement with the experimental observation, as shown in Figures 2 and 3.

Similarly, there is also no driving force for Mg segregating to the Al/Ti interface ($\Delta H_{\text{Ti-Mg}}^{\text{mix}} > 0 > \Delta H_{\text{Al-Mg}}^{\text{mix}}$); this further supports the conclusion that the observed Mg segregation to the Al/Ti interface was not due to the attraction by Ti, but was due to prior oxidation of Mg at the surface of Al.^[20–23]

Using a similar argument, judging from the chemical mixing enthalpies $\Delta H_{X-Y}^{\text{mix}}$, Cu, Fe, and Mn would be expected to segregate to the Al/Ti interface from

Table I. The Chemical Mixing Enthalpies $\Delta H_{X-Y}^{\text{mix}}$ Between the Alloying Elements (Si, V, Cu, Fe, Mn, Ag) and the Matrices (Al,Ti),^[19,35,36] and the Driving Force for Segregating to Al/Ti Interface

System	$\Delta H_{X-Y}^{\text{mix}}$ (KJ/mol)	System	$\Delta H_{X-Y}^{\text{mix}}$ (KJ/mol)	The Driving Force for Segregating to Al/Ti Interface (KJ/mol)	Comment
Al-Ti	-30	Ti-Al	-30	n/a	
Al-Mg	-2	Ti-Mg	16	18	
Al-Si	-19	Ti-Si	-66	-47	
Al-V	-16	Ti-V	-48	32	V is in Ti matrix
Al-Cu	-1	Ti-Cu	-9	-8	
Al-Fe	-11	Ti-Fe	-17	-6	
Al-Mn	-19	Ti-Mn	-27	-8	

thermodynamic considerations alone. However, none of these elements were observed segregated to the interface, as shown in Figure 9. This is probably because the diffusion rates of Cu, Fe, and Mn in Al (see Table II) are relatively slow compared with Si, which has a much smaller atomic size (Table III), since the welding time was very short, only 1.4 seconds, during which the temperature reached ~ 500 °C. In addition according to Table I, the driving force for Cu, Fe, and Mn moving to the interface is much lower than that for Si, which could be another reason for their not being observed to segregate at the interface. It should be noted that in Figure 9, although in the EDS data it looks like there was more Cu, Fe, Mn uniformly distributed on Ti side of the joint, this is likely to be an artifact caused by the

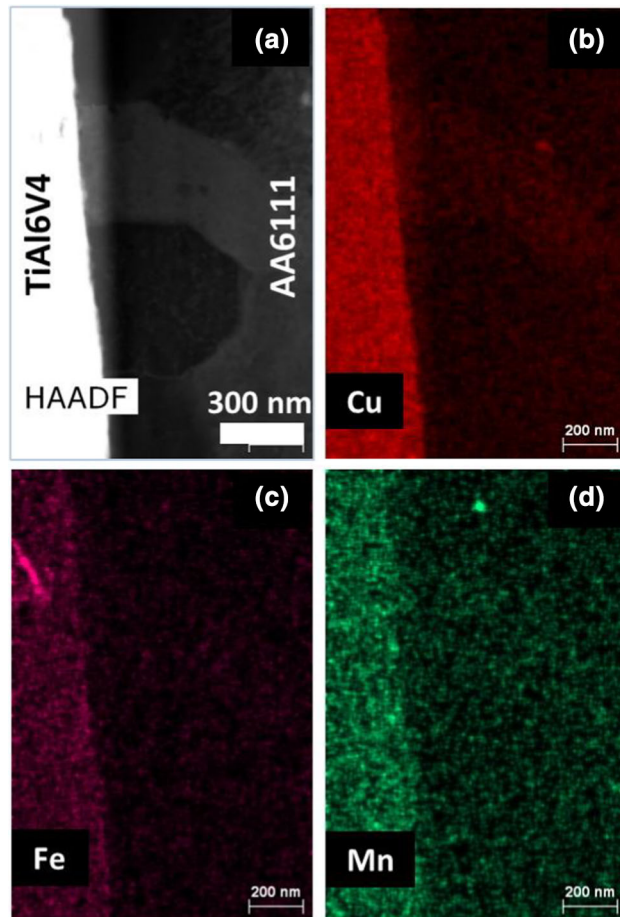


Fig. 9—STEM-EDS element maps in the AA6111/Ti6Al4V interface region, (a) STEM-HAADF image, (b) Cu map, (c) Fe map, (d) Mn map (in the same region with Fig. 2, acquired simultaneously as the data in Fig. 2).

higher atomic number and greater Bremsstrahlung scattering of the Ti matrix compared to Al.

IV. CONCLUSIONS

In the dissimilar ultrasonic welding of Ti6Al4V to AA6111, strong enrichment of silicon, magnesium, and oxygen was found at the as-welded joint interface. In contrast, other alloying elements present, such as Cu and V, were not found segregated to the interface. By high-resolution STEM-EDS analysis, ~ 4 at. pct of Si was found at the Al/Ti interface, distributed in a non-continuous discrete layer ~ 20 nm wide. A simple diffusion model has been used to demonstrate that this layer can potentially form during the rapid UW weld cycle (< 1.4 seconds) even without the requirement of enhanced diffusion, but may also be facilitated by the high strain rate severe deformation generated by the UW process.

It was also interesting to observe that the distribution of segregated Si varied inversely with that of oxygen and magnesium. The observed Mg and O “enrichment” at the Al/Ti weld interface probably originates from residual oxide arising from the broken up oxide film originally on the surface of the AA6111 sheet before ultrasonic welding, due to preferential oxidation of Mg. The lack of observation of any intermetallic reaction in this weld couple, despite the high driving force for forming titanium aluminide phases, suggests that residual oxides and the segregated Si layer at the Al/Ti interface are able to act as a diffusion barrier preventing intermetallic reaction and the nucleation and growth of the Al_3Ti IMC layer.

The strong chemical attraction between Ti and Si, which is characterized by a large great negative enthalpy of chemical mixing between Si and Ti ΔH_{Ti-Si}^{mix} (-66 kJ/mol) is probably the driving force for Si segregation to the Al/Ti interface. It is, however, yet to be determined, if the residual discontinuous oxides at the Al/Ti weld interface and Si-rich layer negatively affect the weld’s mechanical properties.

Table III. Atom Radius^[37]

Element	Al	Ti	Mg	Si	Cu	Fe	Mn
Radius (pm)	118	176	145	111	145	156	161

Table II. Diffusion Coefficient of Various Elements in Aluminum at 500 °C^[34]

Element	Si	Cu	Fe	Mn
Diffusion Coefficient (cm^2/s)	1.5×10^{-9}	5.9×10^{-10}	3.9×10^{-11}	7.5×10^{-13}

ACKNOWLEDGMENTS

This work was funded by the EPSRC through LAT-EST2, Light Alloys towards Environmentally Sustainable Transport (EP/G022402/1) and Friction Joining—Low Energy Manufacturing for Hybrid Structures in Fuel Efficient Transport Applications (EP/G022402/1.JLR). The authors would like to thank Constellium and Airbus UK for the provision of materials and Dr. Y.Q. Chen for help in quantification of EDS data. National Natural Science Foundation of China (Grant Nos. 51605287, U1564204, U1764251), Natural Science Foundation of Shanghai (Grant No. 16ZR1417100), Ministry of Industry and Information Technology of the People's Republic of China (Grant No. 2016ZXFM03002), and China Scholarship Council (CSC, 2011612001) are also gratefully acknowledged for the financial support. Professor Philip B. Prangnell is grateful to the Royal Academy of Engineering, UK, and Airbus for supporting this research through the Airbus-University of Manchester Centre for Metallurgical Excellence. S.J.H. thanks the Engineering and Physical Sciences (U.K.) (Grants EP/M010619/1, EP/P009050/1) and the European Research Council (ERC) under the European Union's Horizon 2020 research and innovation programme (Grant ERC-2016-STG-EvoluTEM-715502).

OPEN ACCESS

This article is distributed under the terms of the Creative Commons Attribution 4.0 International License (<http://creativecommons.org/licenses/by/4.0/>), which permits unrestricted use, distribution, and reproduction in any medium, provided you give appropriate credit to the original author(s) and the source, provide a link to the Creative Commons license, and indicate if changes were made.

REFERENCES

1. A. Panteli, J.D. Robson, I. Brough, and P.B. Prangnell: *Mater. Sci. Eng. A*, 2012, vol. 556, pp. 31–42.
2. Y. Wang, B. Al-Zubaidy, and P.B. Prangnell: *Metall. Mater. Trans. A*, 2018, vol. 49A, pp. 162–76.
3. A. Panteli, J.D. Robson, Y.C. Chen, and P.B. Prangnell: *Metall. Mater. Trans. A*, 2013, vol. 44A, pp. 5773–81.
4. P.B. Prangnell, F. Haddadi, and Y.C. Chen: *Mater. Sci. Technol.*, 2011, vol. 27, pp. 617–24.
5. L. Xu, J.D. Robson, L. Wang, and P.B. Prangnell: *Metall. Mater. Trans. A*, 2018, vol. 49A, pp. 515–26.
6. L. Xu, L. Wang, Y.C. Chen, J.D. Robson, and P.B. Prangnell: *Metall. Mater. Trans. A*, 2016, vol. 47A, pp. 334–46.

7. J.W. Yang, B. Cao, X.C. He, and H.S. Luo: *Sci. Technol. Weld. Join.*, 2014, vol. 19, pp. 500–04.
8. C.Q. Zhang, J.D. Robson, O. Ciuca, and P.B. Prangnell: *Mater. Charact.*, 2014, vol. 97, pp. 83–91.
9. C.Q. Zhang, J.D. Robson, and P.B. Prangnell: *J. Mater. Process. Technol.*, 2016, vol. 231, pp. 382–88.
10. F. Haddadi, D. Strong, and P.B. Prangnell: *JOM*, 2012, vol. 64, pp. 407–13.
11. A. Panteli, Y.C. Chen, D. Strong, X. Zhang, and P.B. Prangnell: *JOM*, 2012, vol. 64, pp. 414–20.
12. J.D. Robson, A. Panteli, and P.B. Prangnell: *Sci. Technol. Weld. Join.*, 2012, vol. 17, pp. 447–53.
13. A. Fuji, K. Ameyama, and T.H. North: *J. Mater. Sci.*, 1995, vol. 30, pp. 5185–91.
14. H. Zhao, M. Yu, Z. Jiang, L. Zhou, and X. Song: *J. Alloys Compd.*, 2019, vol. 789, pp. 139–49.
15. FEI. FEI application note AN0027 07-2010: ChemiSTEM™ technology a revolution in EDX analytics. <http://www.fei.com>.
16. C.E. Caicedo-Martinez, G.E. Thompson, and E.V. Koroleva: *Surf. Eng.*, 2002, vol. 18, pp. 145–50.
17. S.V. Divinski, G. Reglitz, H. Rösner, Y. Estrin, and G. Wilde: *Acta Mater.*, 2011, vol. 59, pp. 1974–85.
18. T. Takemoto and I. Okamoto: *J. Mater. Sci.*, 1988, vol. 23, pp. 1301–08.
19. A. Takeuchi and A. Inoue: *Mater. Trans. JIM*, 2000, vol. 41, pp. 1372–78.
20. X.-Y. Liu, P.P. Ohotnickiy, J.B. Adams, C.L. Rohrer, and R.W. Hyland, Jr: *Surf. Sci.*, 1997, vol. 373, pp. 357–70.
21. H. Deng, W. Hu, X. Shu, and B. Zhang: *Appl. Surf. Sci.*, 2004, vol. 221, pp. 408–14.
22. J. Bloch, D.J. Bottomley, J.G. Mihaychuk, H.M. van Driel, and R.S. Timsit: *Surf. Sci.*, 1995, vol. 322, pp. 168–76.
23. W. Wang, P. Liu, and L. Gan, In *Advanced Materials Research* (2011), pp 157–62.
24. DJ Field, GM Scamans, and EP Butler: *Metall. Trans. A*, 1987, vol. 18A, pp. 463–72.
25. J. Magin and F. Balle: *Mater. Werkst.*, 2014, vol. 45, pp. 1072–83.
26. T. Shimozaki, T. Okino, M. Yamane, Y. Wakamatsu, and M. Onishi, In *Defect and Diffusion Forum*, 1997, pp. 591–96.
27. F. Van Loo and G. Rieck: *Acta Metall.*, 1973, vol. 21, pp. 61–71.
28. D.M. Rodrigues, A. Loureiro, C. Leitao, R.M. Leal, B.M. Chaparro, and P. Vilaça: *Mater. Des.*, 2009, vol. 30, pp. 1913–21.
29. H.J. Liu, Y.C. Chen, and J.C. Feng: *Scripta Mater.*, 2006, vol. 55, pp. 231–34.
30. X. Hou, X. Yang, L. Cui, and G. Zhou: *Mater. Des.*, 2014, vol. 53, pp. 106–17.
31. Y.S. Sato, H. Takauchi, S.H.C. Park, and H. Kokawa: *Mater. Sci. Eng. A*, 2005, vol. 405, pp. 333–38.
32. B. Predel, In *Pu-Re—Zn-Zr*, ed. O. Madelung (Springer Berlin Heidelberg: Berlin, 1998), pp 1–3.
33. C.L. Yeh, W.H. Chen, and C.C. Hsu: *J. Alloys Compd.*, 2007, vol. 432, pp. 90–95.
34. E.A. Association, *EAA*, available at 2013.
35. X.Q. Chen, V.T. Witusiewicz, R. Podlucky, P. Rogl, and F. Sommer: *Acta Mater.*, 2003, vol. 51, pp. 1239–47.
36. Z. Bian, H. Kato, C. Qin, W. Zhang, and A. Inoue: *Acta Mater.*, 2005, vol. 53, pp. 2037–48.
37. E. Clementi, D.L. Raimondi, and W.P. Reinhardt: *J. Chem. Phys.*, 1967, vol. 47, pp. 1300–07.

Publisher's Note Springer Nature remains neutral with regard to jurisdictional claims in published maps and institutional affiliations.